Article

Enhancing Visible-Light Photocatalysis with Pd(II) Porphyrin-Based TiO$_2$ Hybrid Nanomaterials: Preparation, Characterization, ROS Generation, and Photocatalytic Activity

Dawid Malec [1], Marta Warszyńska [1,2], Paweł Repetowski [1,2] , Anton Siomchen [1] and Janusz M. Dąbrowski [1,*]

[1] Faculty of Chemistry, Jagiellonian University, 30-387 Kraków, Poland; dawiid.malec@student.uj.edu.pl (D.M.); m.warszynska@doctoral.uj.edu.pl (M.W.); pawel.repetowski@doctoral.uj.edu.pl (P.R.); anton.siomchen@student.uj.edu.pl (A.S.)

[2] Doctoral School of Exact and Natural Sciences, Jagiellonian University, 30-348 Kraków, Poland

* Correspondence: jdabrows@chemia.uj.edu.pl; Tel.: +48-12-686-2488; Fax: +48-12-686-2750

Abstract: Novel hybrid TiO$_2$-based materials were obtained by adsorption of two different porphyrins on the surface of nanoparticles—commercially available 5,10,15,20-tetrakis(4-sulfonatophenyl)porphyrin (TPPS) and properly modified metalloporphyrin—5,10,15,20-tetrakis(2,6-difluoro-3-sulfophenyl)porphyrin palladium(II) (PdF$_2$POH). The immobilization of porphyrins on the surface of TiO$_2$ was possible due to the presence of sulfonyl groups. To further elevate the adsorption of porphyrin, an anchoring linker—4-hydroxybenzoic acid (PHBA)—was used. The synthesis of hybrid materials was proven by electronic absorption spectroscopy, dynamic light scattering (DLS), and photoelectrochemistry. Results prove the successful photosensitization of TiO$_2$ to visible light by both porphyrins. However, the presence of the palladium ion in the modifier structure played a key role in strong adsorption, enhanced charge separation, and thus effective photosensitization. The incorporation of halogenated metalloporphyrins into TiO$_2$ facilitates the enhancement of the comprehensive characteristics of the investigated materials and enables the evaluation of their performance under visible light. The effectiveness of reactive oxygen species (ROS) generation was also determined. Porphyrin-based materials with the addition of PHBA seemed to generate ROS more effectively than other composites. Interestingly, modifications influenced the generation of singlet oxygen for TPPS but not hydroxyl radical, in contrast to PdF$_2$POH, where singlet oxygen generation was not influenced but hydroxyl radical generation was increased. Palladium (II) porphyrin-modified materials were characterized by higher photostability than TPPS-based nanostructures, as TPPS@PHBA-P25 materials showed the highest singlet oxygen generation and may be oxidized during light exposure. Photocatalytic activity tests with two model pollutants—methylene blue (MB) and the opioid drug tramadol (TRML)—confirmed the light dose-dependent degradation of those two compounds, especially PdF$_2$POH@P25, which led to the virtually complete degradation of MB.

Keywords: metal complexes; porphyrin; reactive oxygen species (ROS); singlet oxygen; titanium dioxide (TiO$_2$)

1. Introduction

The generation of reactive oxygen species (ROS) is an important aspect of not only biological and biochemical processes but also environmental processes [1]. Moreover, ROS play a key role in other applications such as photodynamic therapy of cancer (PDT) [2], photodynamic inactivation of microorganisms (PDI) [3], as well as photodegradation of dyes, drugs, polymers, and various organic compounds. In the ever-expanding field of heterogenous photocatalysis, there is great interest in developing new hybrid materials capable of efficiently activating small molecules [4]. Porphyrins, as the most extensively studied tetrapyrrolic compounds, are well-known photogenerators of ROS [5]. They strongly absorb light from the visible range, which is associated with π–π* electron transitions, and

the energy thereby absorbed is converted into various photophysical processes and photochemical reactions. Therefore, research on porphyrins includes not only photomedicine but also optoelectronics, photocatalysis, and solar energy conversion [6,7].

Porphyrins can coordinate metal ions, which significantly modify their spectroscopic, photophysical, and photochemical properties. Incorporation of various metal ions into the center of the compound also affects their stability, hydrophilicity, and tendency to aggregation, which, in sum, affects the efficiency of photo-oxidation processes [8–10]. Modification of the structure of porphyrins with substituents also has a significant impact on their solubility, stability, and photochemical properties [11,12]. Previous studies have shown that halogenated tetrapyrroles exhibit much higher spin-orbit coupling constants than unmodified analogues, which increases the quantum yield of the intersystem crossing (ISC) [13]. Modification by the attachment of thioester or sulfonamide groups, on the other hand, introduces a steric hinge that increases the overall stability of the molecule [14].

In recent years, metal oxide nanoparticles have garnered widespread interest from researchers in various fields (biomedicine, bioimaging, biosensors, and catalysis) due to their unique physical and chemical properties [15–19]. TiO_2—an n-type semiconductor—is one of the most intensively investigated catalysts, characterized by low toxicity accompanied by its high photochemical and thermal stability and strong oxidizing capability [20–23]. For this reason, it is widely used in biomedical research but also in environmental applications, e.g., as a catalyst in air or water purification [24–28]. It is also used in self-cleaning surfaces, in CO_2 reduction [29,30], in H_2 generation [31], and in the catalytic decomposition of harmful organic compounds [32–35]. The development of nanomaterials has allowed for the improvement of their properties, including the increase in the absorbing material's band gap in the ultraviolet range. However, there is a large bandgap of TiO_2 (E_g = 3.2 eV for anatase, E_g = 3.0 eV for rutile) that determines its limited (ca. 5%) ability to harvest natural sunlight [36–38]. Those disadvantages can be overcome with different modifications such as metal/non-metal doping, co-doping, and sensitization with organic dyes [36–42]. The latter, however, does not function as photocatalysts but will contribute to the hybrid material by leveraging their unique properties. The photosensitization of the materials is based on the sensitizer adsorption to the semiconductor surface and the absorption of photons of an appropriate wavelength, which transition into an excited state. The primary purpose of the sensitizer is to overcome the inherent limitations of inorganic semiconductors [43]. In this paper, we will focus on the photosensitization of TiO_2 with properly designed porphyrin derivatives.

One of the most important features of titanium (IV) oxide is its importance in advanced oxidation processes (AOP), which are related to efficient ROS generation [44]. During the activation of TiO_2 particles with light from the UV range, electrons and holes in the conduction and valence bands are generated [45,46]. The generated charges take part in the oxidation and reduction reactions that occur on the TiO_2 surface [47]. In the case of ROS generation, electrons and holes react with water and O_2 adsorbed on the surface, resulting in the formation of hydroxyl radicals and superoxide ion radicals [48]. This phenomenon can be used, among others, in the photodynamic inactivation of microorganisms, as ROS generated in this way react with biological structures such as lipids, proteins, or DNA, leading to their damage [49]. The best photocatalytic activity of TiO_2 is obtained for anatase or a mixture of anatase and rutile [50]. Titanium (IV) oxide is distinguished from other semiconductors by the long lifetime of the generated hole-electron pairs, which further increases the efficiency of the subsequent photochemical reactions [51]. In addition, substances with anchor groups such as -OH, -COOH, and -SO_3H, phosphates, and metal ions (such as Zn^{2+} and Pd^{2+}) bind well to its surface, further stabilizing the semiconductor-modifier system [49].

Nowadays, numerous organic pollutants from industrial sources, such as synthetic dyes, pesticides, pharmaceuticals, and solvents, pose a serious threat to both the environment and human well-being, especially through water resources. Methylene blue (MB), an artificial cationic dye, is widely used in various industries such as textiles, cosmetics, leather,

and pulp, making it a major contributor to wastewater pollution. It is present not only in wastewater from its industry but also in wastewater from other sectors. Human overexposure to MB has been linked to health issues, including tissue degradation, nausea, shock, and an irregular heartbeat. Consequently, a few techniques have been developed to eliminate these contaminants from water and wastewater to limit their impact on human health and the environment [52,53]. Among various approaches, photocatalytic applications have gained considerable popularity to address these challenges. Metal oxide nanoparticles are widely used in the photocatalytic degradation of these organic pollutant dyes, providing an effective means of remediation. TiO_2 is the most suitable photocatalytic compound due to its superior photocatalytic activity over a wide temperature and pH range [54,55]. Other hybrid materials can also be used for photocatalytic degradation of various pollutants, such as the perylene imide/Bi_2WO_6 hybrid photocatalyst used for the degradation of Bisphenol A. The polymeric compound facilitates the charge separation of carriers, increasing the activity of Bi_2WO_6 [56]. MB is extensively used as a model pollutant in photocatalytic tests, and the process of its degradation is well documented. TiO_2-based photocatalysis may lead to the successful oxidation of dyes, resulting in the mineralization of carbon, sulfur, and nitrogen into CO_2, SO_4^{2-}, $NH4^+$, and NO_3^- [57]. However, MB as a model pollutant can pose some problems. It has been observed that during irradiation with UV radiation, MB molecules undergo desorption from the surface of the catalyst. The initial concentration of the dye has an impact on the rate of the photodegradation reaction. High concentrations of MB can even suppress the degradation process [58]. The photodegradation process of MB is also significantly slower under visible than UV irradiation [59].

In our study, we focused on understanding the physicochemical changes in TiO_2 (P25) after anchoring porphyrins on the surface of nanoparticles and the effects of palladium ion incorporation on the photochemistry of hybrid materials. For our research, we used two different porphyrins—commercially available non-metallic porphyrin—5,10,15,20-tetrakis(4-sulfonatophenyl)porphyrin (TPPS) and synthesized porphyrin complexed with Pd^{2+}-5,10,15,20-tetrakis(2,6-difluoro-3-sulfophenyl)porphyrin palladium (II) (PdF_2POH). These porphyrins were anchored with sulfonic groups to the titanium (IV) oxide surface. Palladium (II) itself also helps to anchor the porphyrin to the TiO_2 surface. In addition, the effect of 4-hydroxybenzoic acid (PHBA) as a linker to increase the amount of attached porphyrin to the TiO_2 surface was also studied. Introducing PHBA on the P25 surface could potentially lead to increased stability of the resulting composite, thus increasing photocatalytic activity [60]. Moreover, the presence of palladium ions in porphyrin-based materials resulted in increased photoinduced charge separation compared to metal-free or zinc derivatives [61,62]. To confirm the adsorption of porphyrins on the P25 surface, UV-Vis electronic absorption measurements were conducted, along with nanoparticle size evaluation and ζ-potential analysis by DLS. We investigated the photosensitization of TiO_2-based materials by photocurrent measurements and ROS generation changes with the use of two probes: singlet oxygen sensor green (SOSG), which is a selective $^1O_2$ probe, and 3′-(*p*-aminophenyl) fluorescein (APF), selective for hydroxyl radical. Finally, we investigated the photocatalytic properties of the obtained materials with two model pollutants—dye methylene blue and an example of an opioid drug—tramadol hydrochloride.

2. Results

2.1. Spectroscopic Characterization of Photosensitizers

Our research starting point was porphyrins such as 5,10,15,20-tetrakis(4-sulfonatophenyl)porphyrin—TPPS or halogenated 5,10,15,20-tetrakis(2,6-difluoro-3-sulfophenyl)-porphyrin—F_2POH (previously described in some of our articles) [49]. However, metal-free porphyrins tend to aggregate in aqueous solutions [63]. By introducing sulfonyl groups, the solubility of the porphyrin can be controlled, leading to changes in spectroscopic properties and the possibility of J-type aggregation, depending on concentration and pH value [64]. To prevent this undesirable process, which can hinder the generation of ROS and reduce activity, we utilized porphyrin derivatives with electron-withdrawing groups. Specifically,

the incorporation of fluorine atoms at the ortho-position of the phenyl rings significantly decreases aggregation, influences the redox properties, and stabilizes the porphyrin structure against (photo)oxidation. Moreover, in this work, we incorporated the Pd^{2+} ion into the halogenated porphyrin structure, which increases the triplet quantum yield and, therefore, enhances the generation of reactive oxygen species. The synthesis of porphyrins was conducted according to the protocols published before [65].

The ground-state electronic absorption spectra of TPPS and PdF_2POH were recorded at room temperature in Tris buffer (pH = 7.4) and are presented along with their chemical structures in Figure 1. The studied porphyrins exhibit characteristic absorptions in the 500–700 nm range (Q-bands), corresponding to electronic transitions between the $S_0 \rightarrow S_1$ states. The addition of Pd^{2+} into the porphyrin ring resulted in the broadening of the Soret band and a slight hypsochromic shift in the absorption maximum (for TPPS λ_{max} = 413 nm, for PdF_2POH λ_{max} = 404 nm). This is caused by the back-donation from Pd(II) *d*-orbitals to the porphyrin's empty π^*-orbitals, thus raising the energy gap of the electronic transition. This insertion also resulted in a reduction in the number of Q-bands caused by the change in porphyrin symmetry ($D_{2h} \rightarrow D_{4h}$). The intense absorption in the blue range (Soret band) for both TPPS and PdF_2POH enables TiO_2 sensitization to the visible region of the spectrum. In addition, the adsorption of porphyrins on the P25 surface should increase charge separation and result in an enhanced amount of photogenerated ROS.
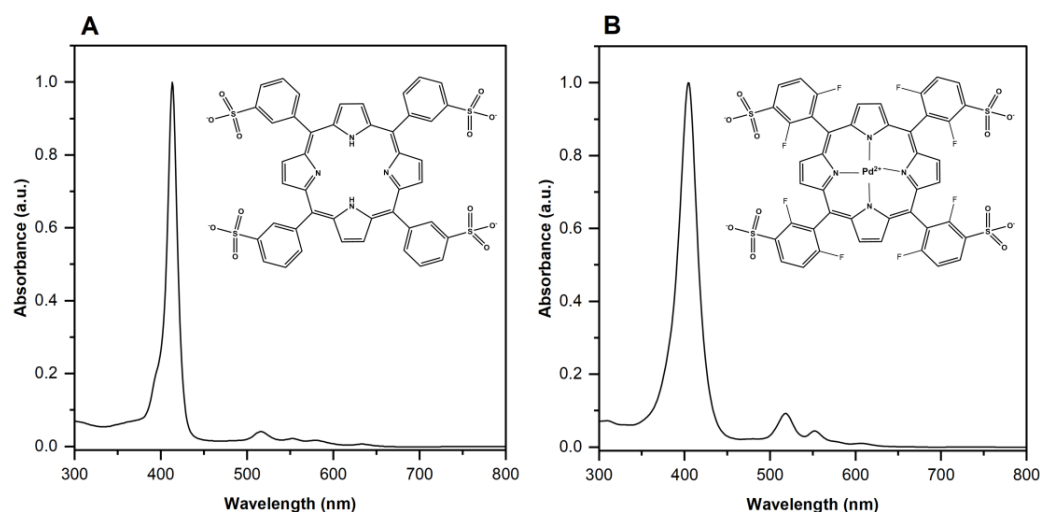

Figure 1. Chemical structure and electronic absorption spectra of 5,10,15,20-tetrakis(4-sulfonatophenyl)porphyrin (TPPS) (**A**) and 5,10,15,20-tetrakis(2,6-difluoro-3-sulfophenyl)porphyrin palladium(II) (PdF_2POH) (**B**).

2.2. Adsorption of (Metallo) Porphyrins on TiO₂ and Their Spectroscopic Characteristics

TiO_2 (P25) is a white powder characterized by limited absorption of visible light. Thus, we synthesized P25-based materials immobilized with two photosensitizers—TPPS and PdF_2POH. We designed two series of materials—porphyrins on TiO_2 and porphyrins on TiO_2 impregnated with 4-hydroxybenzoic acid (PHBA). The materials were obtained after porphyrin solution sonification and overnight shaking with P25 powder and, optionally, with PHBA. After the adsorption of porphyrins, the powder changed its color from white to beige. The diffuse reflectance spectra of modified TiO_2 with TPPS and PdF_2POH and with the incorporation of PHBA into both porphyrins after Kubelka–Munk function calculation are presented in Figure 2.
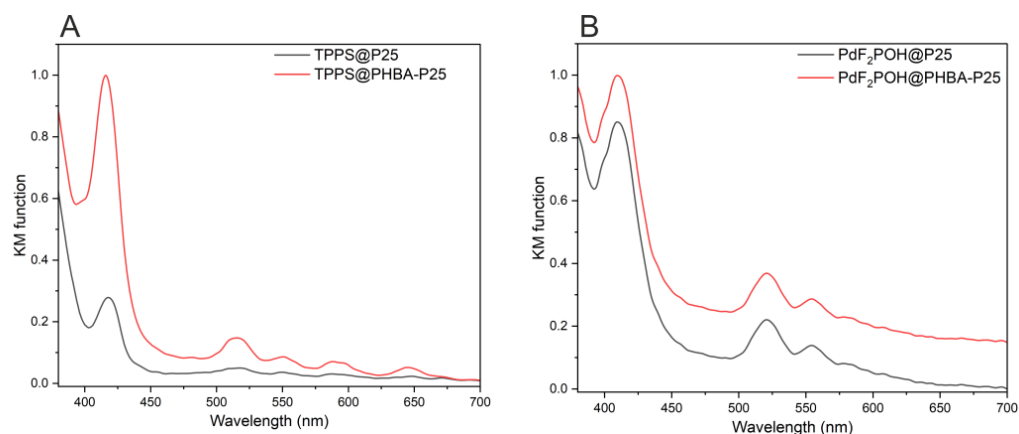
Figure 2. Diffuse reflectance spectra in the representation of the Kubelka–Munk function of TPPS-based materials—TPPS@P25 and TPPS@PHBA-P25 (**A**) and PdF$_2$POH-based materials—PdF$_2$POH@P25 and PdF$_2$POH@PHBA-P25 (**B**).

Electronic absorption spectra confirm the deposition of porphyrins on the TiO$_2$ surface. Bare TiO$_2$ shows no absorption bands above 400 nm. Adsorption of porphyrins on P25 resulted in a red shift of the Soret band (420 nm) compared to unmodified porphyrins (Figure 1), which indicates S$_0$→S$_2$ transitions in all tested compounds, proving a successful synthesis of hybrid TiO$_2$ materials. Figure 2 shows absorption bands in the 400–550 nm range for both TPPS and the palladium (II) derivative.

2.3. Characterization of the Nanomaterials Size and ζ-Potential

To further prove the adsorption of porphyrin on the TiO$_2$ surface, the size of the resulting composites and ζ-potential were defined by dynamic light scattering (DLS) measurements (Figure 3, Table 1). The particle size of modified nanomaterials in aqueous solution possesses a homogeneous distribution, with 146 nm for unmodified P25, and 155 nm, 170 nm, and 197 nm, respectively, for TPPS@P25, TPPS@PHBA-P25, PdF$_2$POH@P25 and PdF$_2$POH@PHBA-P25. The dispersion stability of synthesized hybrid material nanoparticles is characterized by zeta potential (ζ). The obtained values for ζ-potential varied for different formulations. P25 showed a positive potential on the depletion layer (ζ = 21 mV). The lowest ζ-potential was observed for TPPS@P25 and TPPS@PHBA-P25 (ζ = −9 mV and ζ = −33 mV, respectively). The low surface charge of TPPS@P25 can be explained by the structure of the porphyrin itself—negatively charged sulphonyl groups are the source of negative potential. The addition of an acidic linker—PHBA—further lowers the charge of the depletion layer to −33 mV. However, surface modification with palladium derivatives did not result in a ζ-potential decrease, even a slight increase (ζ = 22 mV), which can be due to the fact that positively charged palladium ions reduce the effects of sulphonyl groups. The addition of 4-hydroxybenzoic acid decreased the ζ-potential value to 12 mV. The ζ-potential measurements suggest that TPPS@PHBA-P25 and PdF$_2$POH@P25 are the most stable of all the composites obtained and are less likely to aggregate in solutions. All determined values are presented in Table 1.

2.4. Photolectrochemical Measurements

TiO$_2$ is a semiconductor capable of generating photocurrents within UV irradiation (>400 nm), as it is characterized by a wide bandgap. The absorption of UV photons leads to electron excitation from the valence to the conduction band. This is represented by the current increase.
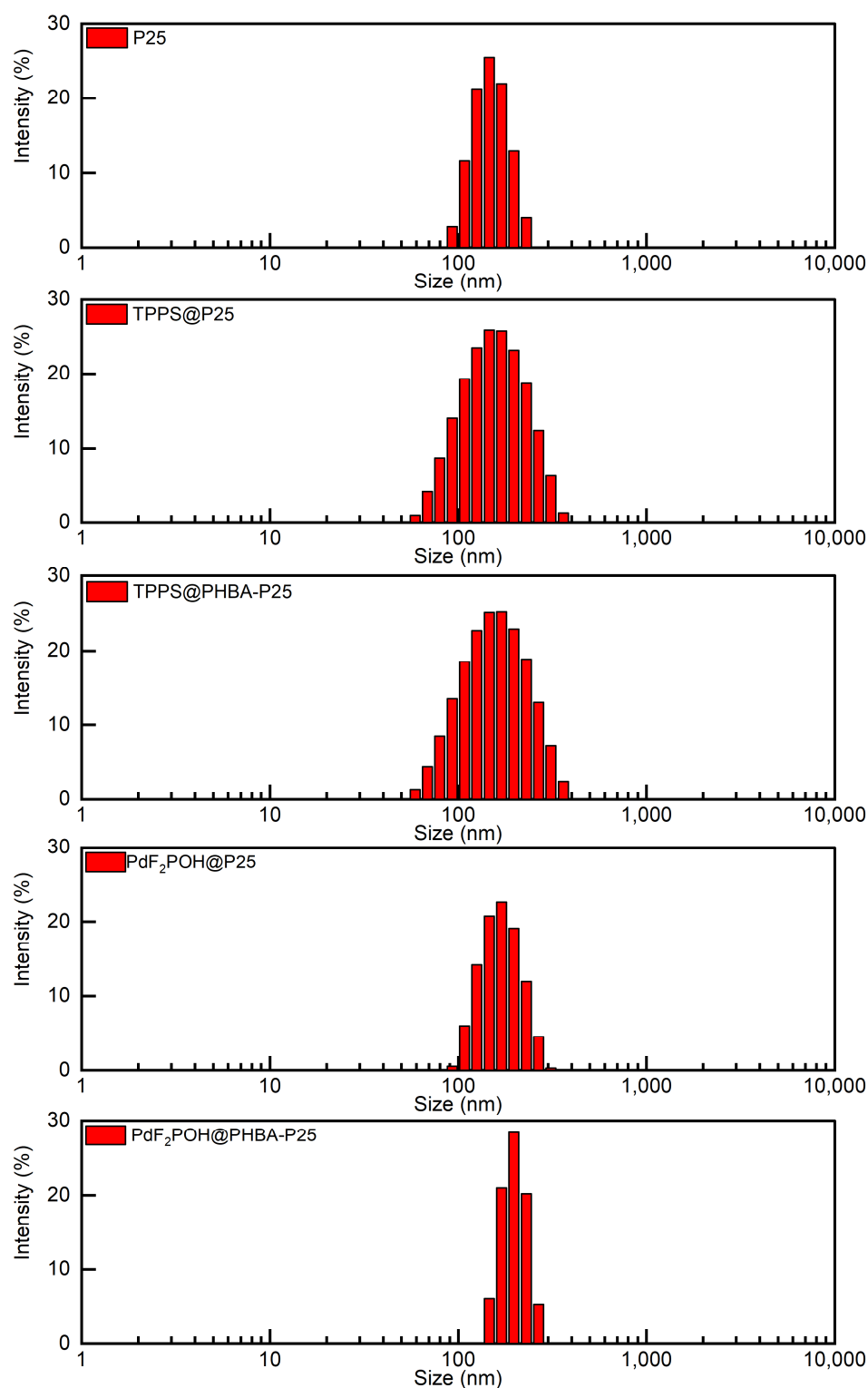
Figure 3. Size distribution of bare P25 and porphyrin-based materials—TPPS@P25, TPPS@PHBA-P25, PdF$_2$POH@P25, and PdF$_2$POH@PHBA-P25.

The detection of photocurrents above 400 nm for PdF$_2$POH@P25, PdF$_2$POH@PHBA-P25, and TPPS@PHBA-P25 confirms that porphyrins sensitize titania to visible light (Figures 4 and 5). Figure 5 presents the photocurrent response to chopping light irradiation. In the case of strongly adsorbed PdF$_2$POH@P25, the photocurrents coincide precisely with the energy levels of the Soret and Q$_{xy}$ absorption bands of the porphyrin adsorbed on

the TiO$_2$ surface. This suggests that both S$_0 \rightarrow$S$_2$ and S$_0 \rightarrow$S$_1$ excitations may contribute to the enhanced photochemical activity of the modified titania. In the case of TPPS@P25, there was negligible to no change in photocurrents above 400 nm (Figures 4A and 5A), suggesting that this modification failed to sensitize P25 to visible light. However, in the UV range (325–400 nm), the intensity of the photocurrent was enhanced in comparison to unmodified P25. Comparing the photocurrent measurement results, it becomes obvious that porphyrins sensitize PHBA-P25 material more effectively than P25, and the cathodic current is generated (Scheme 1). The generation of cathodic photocurrent is a consequence of the oxidation of the dye by the produced species [66]. Previous studies indicate that the lower potential oxidation wave can be attributed to the oxidation of the -SO$_3$H group. The second oxidation wave, potentially consisting of two unresolved peaks, may be associated with the oxidation of the macrocycle. The assigned oxidation potentials are much lower than the valence band edge potential of titanium, which is about 2.7 V at pH = 7 [67]. This suggests that electron transfer from the valence band of TiO$_2$ to the excited dye molecule is unlikely. Given the redox properties of the adsorbed (metallo)porphyrins and P25, the observed visible light-induced photocurrents may be due to electron transfer from the excited dyes to the TiO$_2$ conduction band.

Table 1. Particle size and ζ-potential of the tested nanomaterials.

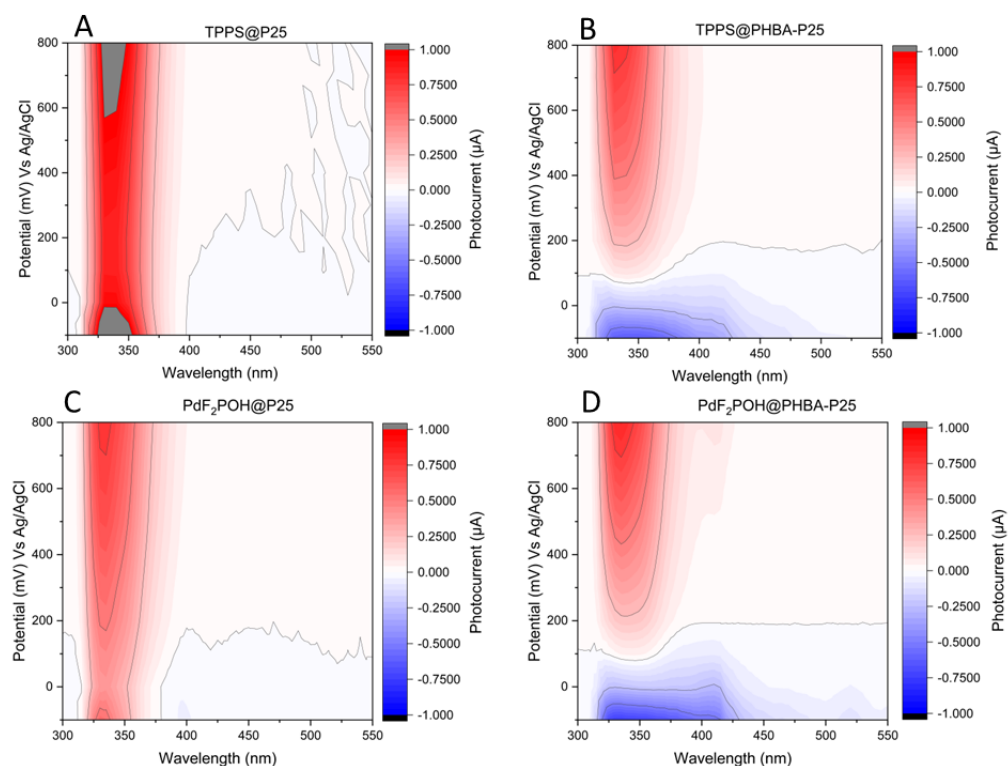| Material	Size/nm DLS	ζ/mV
P25	146	21
TPPS@P25	154	-9
TPPS@PHBA-P25	155	-33
PdF$_2$POH@P25	170	22
PdF$_2$POH@PHBA-P25	197	12

Figure 4. Photocurrent as a function of potential (vs. Ag/AgCl) and incident light wavelength, recorded on ITO electrodes in a 0.1 M KNO$_3$ aqueous solution electrolyte (pH = 7). Photocurrent measure for (**A**) TPPS@P25, (**B**) TPPS@PHBA-P25, (**C**) PdF$_2$POH@P25, (**D**) PdF$_2$POH@PHBA-P25.
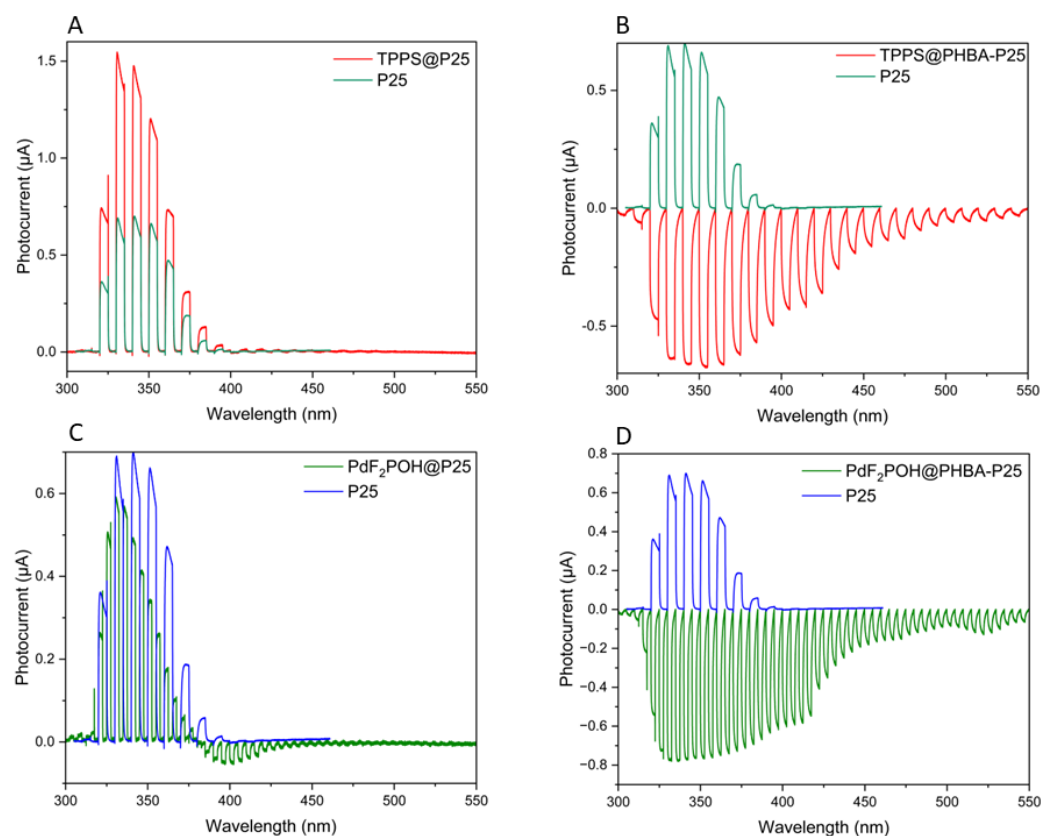
Figure 5. Photocurrents generated by the electrodes covered with P25 and PHBA-P25 with adsorbed (metallo)porphyrins ((**A**)—TPPA@P25, (**B**)—TPPS@PHBA-P25, (**C**)—PdF$_2$POH@P25, (**D**)—PdF$_2$POH@PHBA-P25) as a function of the wavelength of incident light (applied potential -200 mV vs. Ag/AgCl).

Tabari et al. recorded the generation of photocurrent when surface-modified TiO$_2$ remained unchanged under different polarization conditions, whether negative or positive ones [68]. Upon UV irradiation in the studied potential range, pristine TiO$_2$ generates anodic photocurrents. In the case of unmodified TiO$_2$ (Scheme 1a), even under negative polarity, electrons move towards the conductor, since trapping by the redox couple of the electrolyte (e.g., O$_2$) proves ineffective. In contrast, for dye-modified TiO$_2$, additional pathways (as shown in Scheme 1b–d) elucidate the visible light-induced electrochemical behavior. Under negative polarity conditions, excitation by ultraviolet and visible light led to the observation of photocathode currents as electrons moved from the conductor to the oxidized ground state of dye (HOMO).

2.5. Detection of Reactive Oxygen Species in Heterogeneous System

One of the most important features of photosensitizers used in PDT is their ability to generate singlet oxygen (type II photochemical reactions) and other ROS (type I photochemical reactions). To assess whether the adsorption of porphyrins on the TiO$_2$ surface elevated the generation of singlet oxygen (^{1}O$_2$), we used the Singlet Oxygen Sensor Green (SOSG) fluorescent probe (Figure 6). For the hydroxyl radical, we used 3'-(*p*-aminophenyl) fluorescein (APF) (Figure 7). Materials were suspended in PBS in concentrations corresponding to absorbance values of 1. The probes were added to the material suspension with a final concentration of probe 50 μM. Prepared solutions were irradiated with LED light at wavelength λ = 420 ± 20 nm. For TPPS@P25 and TPPS@PHBA-P25, the results indicate a much higher quantum yield of singlet oxygen generation compared to TPPS in the homogenous system. At low light doses (0.1–15 J/cm^2), TPPS@P25 generates singlet oxygen more efficiently; however, at light doses of 20–30 J/cm^2, TPPS@PHBA-P25 has

a higher quantum yield of singlet oxygen generation (Figure 6A). After incorporating the palladium ion into the porphyrin ligand, the mechanism of ROS generation changes in favor of the Type I photochemical reaction mechanism. However, in the case of the palladium derivative, such a large change in the degree of singlet oxygen generation is not observed. On the contrary, at light doses of 0.1–5 J/cm^2, unmodified porphyrin generates singlet oxygen to a greater extent than when applied to TiO$_2$ or TiO$_2$ with PHBA. At higher light doses, both materials as well as unmodified porphyrins generate singlet oxygen to a similar extent, suggesting that the application of PdF$_2$POH to the composite material does not enhance the generation of ^{1}O$_2$ (Figure 6B).
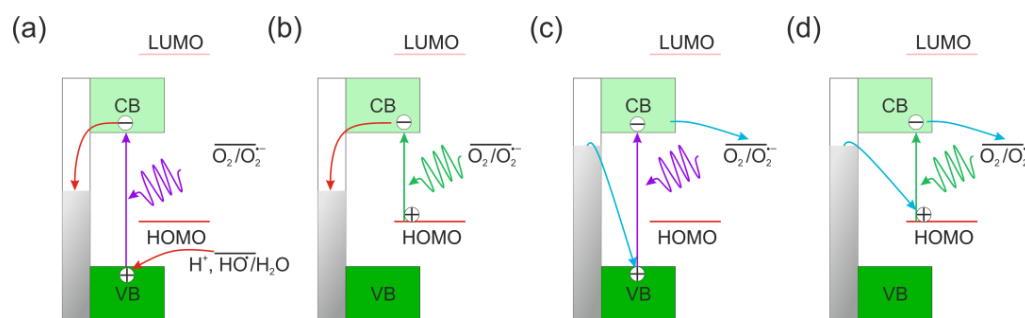
Scheme 1. Photocurrent generation mechanism based on [69]: anodic photocurrents originate from positive potential of TiO$_2$ excitation (**a**) or excitation of the dye (**b**), cathodic photocurrents are generated upon excitation of TiO$_2$ at potentials with negative values (**c**) or by the excitation of complex between the dye and the surface of the material (**d**). The vertical bar indicates the value of photoelectrode potential, and the arrows indicate the transition of electrons from the valence or conduction bands.
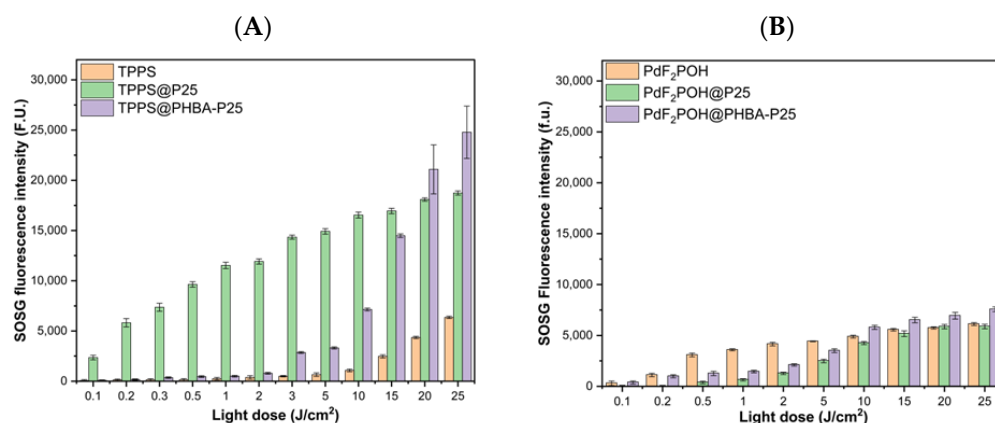

Figure 6. Photogeneration of singlet oxygen. Light dose-dependent increase in fluorescence generated by fluorescent probe—SOSG in the presence of TPPS-based materials (**A**) and PdF$_2$POH-based materials (**B**) irradiated with 420 ± 20 nm.

For hydroxyl radical generation, the results show an inverse relationship. In the case of unmodified TPPS, hydroxyl radical generation was relatively low for all light doses used. The utilization of TiO$_2$-based material and PHBA enhanced type I mechanism reactions only slightly (Figure 7A). The unmodified palladium derivative generates HO· at a higher degree than singlet oxygen, especially at higher light doses (5–30 J/cm^2). PdF$_2$POH deposition has virtually no effect on hydroxyl radical generation efficiency, but the addition of PHBA significantly increases their production. Differences become apparent at light doses higher than 2 J/cm^2. At a light dose of 30 J/cm^2, an almost three times higher signal was achieved for PdF$_2$POH@PHBA-P25 than for palladium porphyrin alone or porphyrin deposited on unmodified P25 (Figure 7B).
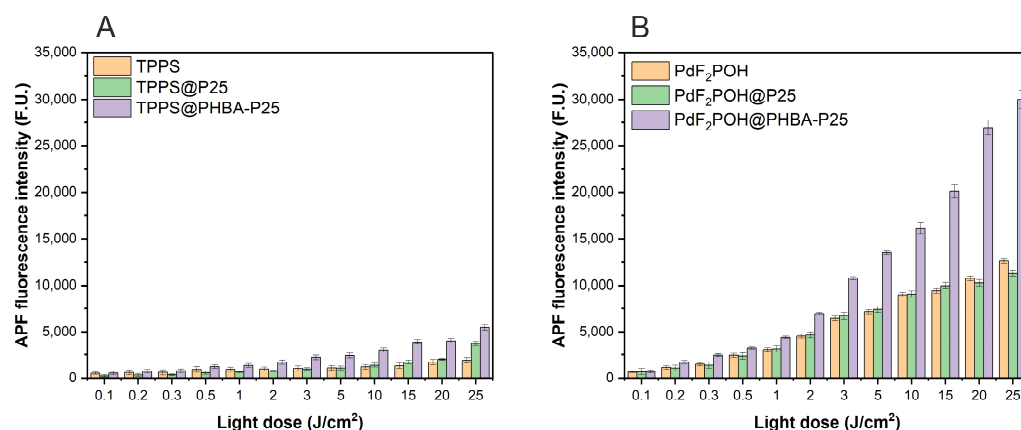
Figure 7. Photogeneration of hydroxyl radicals. Light dose-dependent increase in fluorescence generated by the fluorescein (product of APF reaction with hydroxyl radical) in the presence of TPPS-based materials (**A**) and PdF_2POH-based materials (**B**) irradiated with 420 ± 20 nm.

The increased fluorescence of fluorescein, which is a product of the APF reaction with hydroxyl radical for $PdF_2POH@PHBA$-P25, and the small fluorescence signal of the SOSG probe suggest that this material enhances the generation of reactive oxygen species by mechanism I photochemical reactions. Nosaka et al. proposed a mechanism for TiO_2 systems in which the reverse electron transfer occurs from a superoxide ion formed after the one-electron reduction in dioxygen by e_{CB}^- to the valence band hole or a hole trapped on the TiO_2 surface [70]. This mechanism was suggested because, under these irradiation conditions, the efficient production of holes is less probable. For photocatalytic purposes, the most optimal would be if the materials generated ROS by two photochemical reactions—$^1O_2$ and OH. Furthermore, it would be beneficial to measure other ROS, such as H_2O_2, and $O_2^{\cdot-}$ to obtain a broad image of the photocatalytic reaction for the hybrid materials.

2.6. Photodegradation Studies

In environmental applications, it is important for the materials to be sufficiently photostable. Photostability tests were conducted for solid TPPS@P25, TPPS@PHBA-P25, $PdF_2POH@P25$, and $PdF_2POH@PHBA$-P25 materials mixed with barium sulfate ($BaSO_4$) in a ratio of 1:10. Diffuse reflectance spectra of the materials were recorded after the irradiation ($\lambda = 420 \pm 20$ nm) with the described light doses. The spectra were captured both prior to and immediately after the irradiation, with a time window of 10 to 120 min. Changes in the absorption spectra upon irradiation at 420 nm showed their reduced photochemical stability (Figure 8). The photostability of TPPS@P25, $PdF_2POH@P25$, and $PdF_2POH@PHBA$-P25 was quite similar. However, palladium-containing materials exhibited the greatest stability. The addition of PHBA to the TPPS-based hybrid material decreased its stability. These results can be connected to the high generation of singlet oxygen by TPPS@PHBA-P25 (Figure 6A). After irradiation with light doses over 5 J/cm^2, this porphyrin generates a significant amount of singlet oxygen, which probably oxidizes the material, decreasing its photostability.

2.7. Photocatalytic Degradation of Methylene Blue and Tramadol Hydrochloride in a Heterogenous System

Several researchers investigated the photocatalytic performance of hybrid (metallo)-porphyrin-TiO_2 materials and their adaptable capabilities in electron or energy transfer reactions when exposed to visible light. These materials were examined using model pollutant molecules (such as methyl orange and 4-nitrophenol) and pharmaceutical compounds. The photocatalytic activity of our porphyrin@TiO_2 hybrid materials was examined towards methylene blue dye (MB) and tramadol hydrochloride (TRML) degradation. The experiments have been performed using continuous white light emitted by an Xe lamp

(XBO-150) equipped with a 400 nm cut-on filter for both compounds and, additionally, a 505 nm cut-off filter for MB. Our porphyrin-based materials are perfect for photocatalytic degradation of MB as they absorb in the range of 350–500 nm; therefore, it is possible to avoid the absorption of this model pollutant. The electronic absorption spectra of these two model pollutants, along with their chemical structure, are presented below (Figure 9).
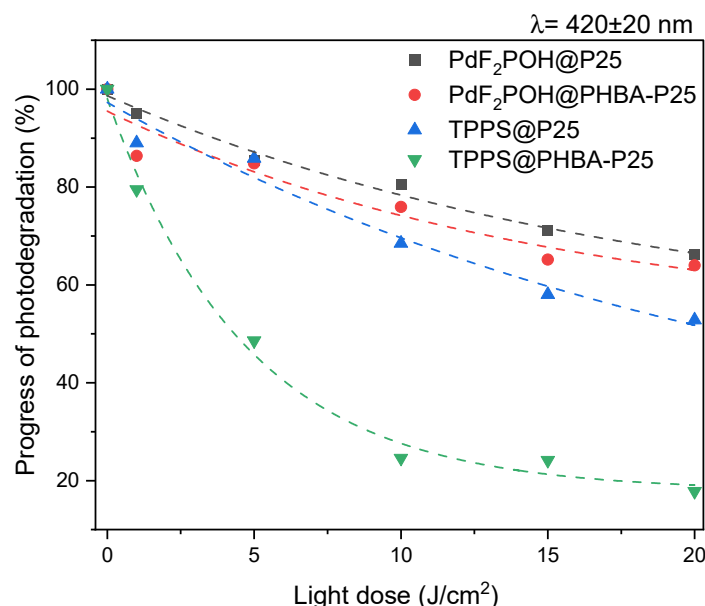

Figure 8. Photodegradation of TiO$_2$-modified materials (TPPS@P25, TPPS@PHBA-P25, PdF$_2$POH@P25, and PdF$_2$POH@PHBA-P25 upon irradiation with visible light (>400 nm).
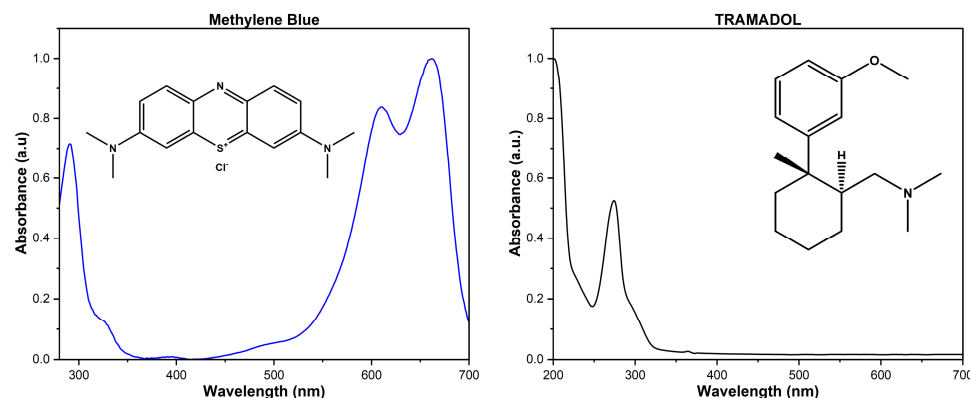

Figure 9. Electronic absorption spectra and chemical structures of two model pollutants—methylene blue (**left**) and tramadol (**right**).

Results of MB photodegradation tests suggest better photocatalytic activity for PdF$_2$POH@P25, than for the rest of the tested materials (Figure 10). In the case of PdF$_2$POH@P25, we observed almost complete degradation of MB. It is also probable that PdF$_2$POH@PHBA-P25 would catalyze full degradation of MB with higher light doses than used in the experiment, similar to TPPS@P25. In the case of TRML, TPPS@P25, and PdF$_2$POH@PHBA-P25 exhibited similar activity, showing almost 70% of TRML degradation after irradiation with a light dose of 6 J/cm^2 (Figure 11). Modification of TPPS-based material showed improvement in photocatalytic activity after incorporation of PHBA into the nanoparticle structure, resulting in almost 90% degradation of MB; however, such a result was not observed for TRML photodegradation [71]. For the latter, TPPS@P25 degraded TRML at 60% after irradiation with a 3 J/cm^2 light dose. The addition of PHBA reduced the degradation of TRML to 20% after the same dose of light. On the other hand, the addition of PHBA increased the photocatalytic activity of PdF$_2$POH-based materials. TPPS@PHBA-P25 exhibited good photocatalytic activity towards MB degradation at lower light

doses (1–8 J/cm^2), but in the end, showed similar activity to the rest of the materials. For TRML degradation, the final result was similar for all tested materials, reaching the degradation of 70–80% of the compound [72]. The results of the tramadol photodegradation tests suggest better photocatalytic activity than the materials we tested previously (F$_2$PMet@TiO$_2$, ZnF$_2$Pmet@TiO$_2$, and CoF$_2$Pmet@TiO$_2$- as described earlier by some of us) [73].

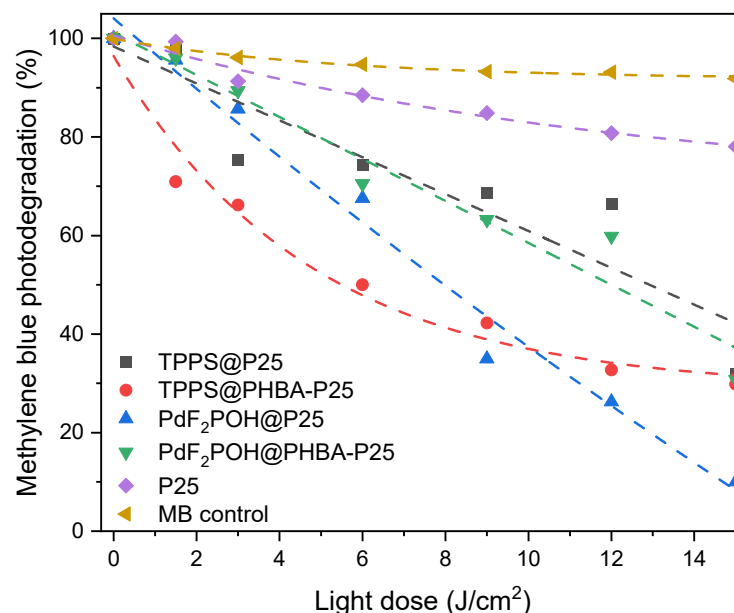**Figure 10.** Photodegradation of methylene blue (MB) in presence of various TiO$_2$-modified materials: TPPS-based (TPPS@P25, TPPS@PHBA-P25), PdF$_2$POH-based (PdF$_2$POH@P25, PdF$_2$POH@PHBA-P25), unmodified P25, and methylene blue as a control upon irradiation with visible light (with cut-on filter > 400 nm and cut-off filter < 520 nm).
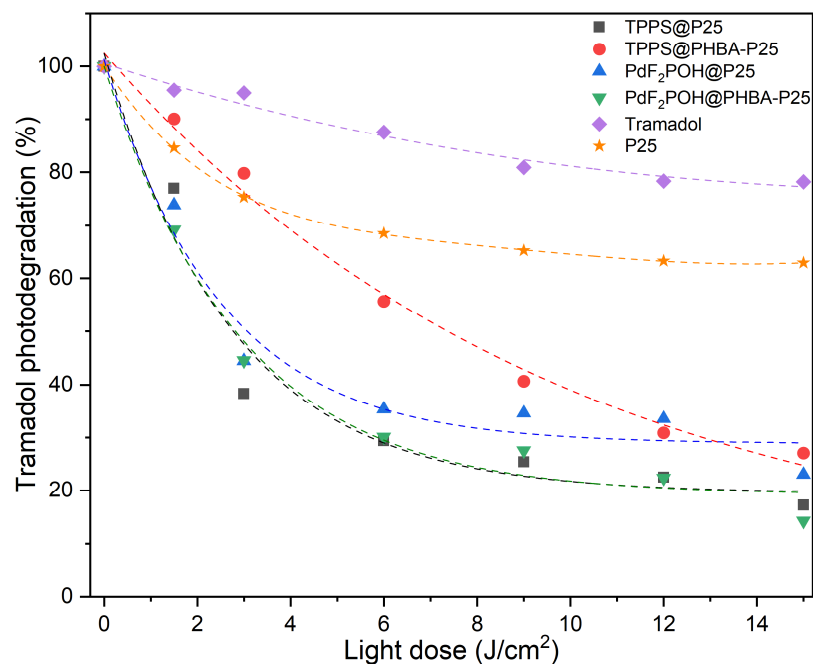

Figure 11. Photodegradation of tramadol (TRML) in the presence of various materials such as TPPS-based (TPPS@P25, TPPS@PHBA-P25), PdF$_2$POH-based (PdF$_2$POH@P25, PdF$_2$POH@PHBA-P25), unmodified P25, and tramadol as a control upon irradiation with visible light (with cut-off filter > 400 nm).

MB alone has shown little photodegradation under visible light; however, with TiO_2, it was degraded by 80% after irradiation with a light dose of 15 J/cm^2. TRML alone showed a slight photodegradation at light doses over 6 J/cm^2, which was enhanced by TiO_2 catalysis.

3. Discussion and Conclusions

Inorganic semiconductors present numerous futures for their applications in environmental, biological, and medical fields. TiO_2 has garnered particular interest due to its distinctive attributes, including its classification as a wide-band gap semiconductor, biocompatibility with living systems, water stability, and pronounced photocatalytic efficacy. Significantly, TiO_2 also allows for surface modification through various inorganic and organic molecules, such as tetrapyrrolic and tetraindolic compounds, facilitating the creation of hybrid composites capable of expanding the photoactivity of TiO_2 to encompass the visible light spectrum. One such modification can be the adsorption of porphyrins widely used in photodynamic therapy and the photodynamic inactivation of microorganisms. The TiO_2 surface can also be modified with anchoring compounds such as 4-hydroxybenzoic acid (PHBA), which increases the number of porphyrin molecules binding to the surface of nanoparticles.

In our work, we investigated the photochemical properties of newly synthesized porphyrin-based materials—with commercially available porphyrin—TPPS and synthesized by us, never studied before metalloporphyrin—PdF_2POH. We used a novel approach in the preparation of porphyrin-based composites by impregnation with 4-hydroxybenzoic acid (PHBA), which serves as a linker for higher adsorption on the TiO_2 surface. Electronic absorption spectra and DLS measurements (size and ζ-potential) prove the effective adsorption of all tested porphyrins on the P25 surface. We managed to successfully sensitize TiO_2 with three of the four prepared materials, which is proven by photoelectrochemical measurements. Our research also proved that the adsorption of porphyrins on the surface of TiO_2 modified the generation of ROS, mainly singlet oxygen for TPPS-based materials and hydroxyl radical for PdF_2POH-based materials. Composites with the addition of PHBA showed higher quantum yields of both singlet oxygen and hydroxyl radicals. The adsorption of TPPS on the P25 surface enhanced the generation of $^1O_2$ but did not cause drastic changes in hydroxyl radical generation. Opposite results were obtained for PdF_2POH—metalloporphyrin-based materials did not influence singlet oxygen generation but increased the production of hydroxyl radicals. The inherent capacity of nanomaterials to facilitate electron transfer, thereby promoting ROS generation, constitutes an intrinsic characteristic of these materials and ensures their effective application as a photocatalyst for multiple purposes. Our findings demonstrate that the surface modification of P25 resulted in the generation of singlet oxygen and hydroxyl radicals, correlating with the physicochemical attributes concerning mechanisms and activity. Moreover, PdF_2POH leads to the generation of a higher amount of ROS compared to previously synthesized $F_2POH@P25$ and $ZnF_2POH@P25$. The incorporation of PHBA into the structure of the composite enhanced the generation of singlet oxygen for TPPS-based material and hydroxyl radical for PdF_2POH-based material.

Palladium (II) porphyrin-based materials—$PdF_2POH@P25$ and $PdF_2POH@PHBA$-P25—were more photostable than materials synthesized before in our group [49]. Low TPPS@PHBA-P25 photostability can be caused by its high singlet oxygen generation, which can lead to the oxidation of the material and its low stability after irradiation with higher light doses. Therefore, when designing hybrid composites, it is important to balance ROS generation with photostability. High generation of singlet oxygen can lead to oxidation of the material, which limits its photostability and photocatalytic activity. $PdF_2POH@P25$ managed to catalyze the photodegradation process almost to completion. $PdF_2POH@PHBA$-P25 also has the potential to fully catalyze the degradation process, but higher light doses are required. In the case of TRML degradation, all hybrid materials degraded the model drug pollutant by 70–80%. The best results were obtained for TPPS@P25, $PdF_2POH@P25$, and $PdF_2POH@PHBA$-P25 materials, which catalyze photodegradation by 50% after irradiation

with a 3 J/cm^2 light dose. TPPS@PHBA-P25 catalyzed the degradation of TRML slower in comparison to other synthesized materials.

Collectively, the comprehensive investigations conducted in this study affirm that TiO$_2$ nanoparticles, when modified with porphyrins and metalloporphyrins, exhibit photoactivity in the visible light-range, enhanced ROS generation, and potential in visible light-driven photocatalysis. Moreover, all synthesized compounds and materials also have a great promise for the photodynamic inactivation of microorganisms, so further research into their biological activity is currently being undertaken.

4. Materials and Methods

4.1. Physicochemical Properties

4.1.1. Preparation of PHBA-P25 Materials

Degussa P25 TiO$_2$ (1200 mg) and a solution of PHBA (100 mg) in deionized water (20 mL) were mixed and placed in the ultrasonic bath for 1 h. The resulting homogenous mixture was protected from light and shaken overnight. After centrifugation (9000 RPM, 15 min), the solid residue was washed with deionized water (20 mL) and centrifugated again. The bulky yellowish residue was dried at 80 °C for 12 h. After drying, the solid was ground in the agate mortar to obtain PHBA-P25 as a yellow powder. This protocol is a modified version of the protocol from Mahy et al. [60].

4.1.2. Preparation of TPPS/PdF$_2$POH Hybrid Nanomaterials

Here, 500 µM porphyrin solution in DMF (2 mL) and a solution of appropriate TiO$_2$ nanomaterial (200 mg) in Tris buffer (2 mL) was mixed and placed in the ultrasonic bath at 60 °C for 2 h. The resulting pinkish suspension was protected from light and shaken overnight. After centrifugation (9000 RPM, 15 min), the solid residue was washed with deionized water (5 mL) and centrifugated again. The bulky pale pink residue was dried at 60 °C for 12 h. After drying, the solid was ground in the agate mortar to obtain material powder.

4.1.3. UV-Vis-NIR Electronic Absorption Spectra Measurements

The photosensitizer samples were dissolved in Tris buffer, pH 7.4. UV-Vis absorption spectra were recorded in quartz cuvettes (l = 1 cm) with a UV-3600 Shimadzu UV-Vis-NIR spectrophotometer (Shimadzu, Kyoto, Japan) in the range of 350–700 nm.

4.1.4. Dynamic Light Scattering (DLS)

ζ-potential and hydrodynamic diameter measurements of nanomaterials in colloid materials were performed using Zetasizer Ultra ZS (Malvern Instruments, Malvern, UK). The apparent diffusion coefficients of the nanoparticles were obtained from the normalized time correlation function of the scattered electric field, g(1) (τ), using the cumulants analysis. An average value was obtained from repeated measurements for each sample (N = 5).

4.1.5. Detection of Reactive Oxygen Species Using Fluorescent Probes

3′-(*p*-aminophenyl) fluorescein (APF) and singlet oxygen sensor green (SOSG) probes were employed for the detection of ROS generated during illumination of the colloid materials and photosensitizer itself. The compound absorbance was at a level of about 1.0. Each fluorescent probe was added to a well at a final concentration of 50 µM. Freshly prepared solutions were then irradiated with LED (420 ± 20 nm) light for increasing time intervals. A Tecan Infinite M200 Reader microplate reader was employed to capture the fluorescence signal both immediately before and right after exposure to light. When APF was utilized, a fluorescence signal at 515 nm was detected after excitation at 490 nm. In the case of SOSG, fluorescence emission was observed at 525 nm, with an excitation wavelength of 505 nm.

4.1.6. Photoelectrochemical Measurements

Photocurrents of modified and unmodified TiO_2 were measured using a three-electrode setup with a 0.1 M KNO_3 electrolyte. The working electrode was prepared by spreading the studied material on an ITO-coated transparent foil and drying it with warm air. A platinum wire and Ag/AgCl (3 M) were used as the counter and reference electrodes, respectively. Photoelectrochemical experiments were conducted utilizing a consistent potentiostat and a 150 W xenon lamp (Photon Institute, Varanasi, India), featuring an automated monochromator with a shutter (Photon Institute) employed as the illumination source, emitting monochromatic light spanning the entire UV and visible light spectrum. The working electrodes were exposed to irradiation from the rear surface.

4.1.7. Photodegradation Studies

Photodegradation of hybrid materials was monitored by the measurements of the changes in the diffuse reflectance spectra recorded for the materials irradiated with 420 ± 20 nm LED light. The DRS spectra were recorded before and immediately after irradiation with light doses from 1 to 20 J/cm^2 using a Shimadzu (Kyoto, Japan) 3600 UV-Vis-NIR spectrophotometer.

4.1.8. Photocatalytic Activity of the Hybrid Materials

The photocatalytic activity of porphyrin@TiO_2 materials was tested by monitoring the progress of tramadol hydrochloride (TRML) and methylene blue (MB) (both purchased from Sigma-Aldrich, Burlington, MA, USA) photodegradation in Tris solution. Continuous irradiation of a suspension of TiO_2 impregnated with porphyrins (7 mg) in solution of model pollutants (14 mL of both: B: $c_0 = 6.71 \times 10^{-4}$ M, TRML: $c_0 = 17$ mg/L) was carried out using the xenon lamp (XBO-150) equipped with the copper (II) sulfate filter (10 cm optical length) and a 400 cut-on (and 505 nm cut-off filter for MB), delivering 1.7 mW/cm^2. The suspension was stirred and irradiated in a cylindrical quartz cuvette (l = 1 cm). Application of this filter enabled the excitation of hybrid materials in the visible range of electromagnetic radiation without the excitation of neither TRML nor MB. The progress of the reactions indicating pollutant degradation was monitored by the measurements of the electronic absorption spectra of TRML and MB. A UV-3600 Shimadzu UV-Vis-NIR spectrophotometer was used for all of these experiments.

Abbreviations

AOP	Advanced oxidation processes
APF	3′-(p-aminophenyl) fluorescein
CO_2	Carbon dioxide

DLS	Dynamic Light Scattering
DMF	Dimethylformamide
DNA	Deoxyribonucleic acid
DRS	Diffuse reflectance spectroscopy
e_{CB}^-	Relative conduction band
H_2O_2	Hydrogen peroxide
ISC	Intersystem crossing
ITO	Indium Tin Oxide
KNO_3	Potassium nitrate
MB	Methylene blue
OH·	Hydroxyl radicals
$^1O_2$	Singlet oxygen
TPPS	5,10,15,20-tetrakis(4-sulfophenyl)porphyrin
TiO_2	Titanium(IV) oxide
P25	Type of Titanium(IV) oxide, Anatase-Rutile ratio: 85:15
PBS	Phosphate buffered saline
PdF_2POH	Palladium(II) 5,10,15,20-tetrakis(2,6-difluoro-3-sulfophenyl)porphyrin
PDI	Photodynamic inactivation
PHBA	4-hydroxybenzoic acid
ROS	reactive oxygen species
SOSG	Singlet Oxygen Sensor Green
TRML	Tramadol

References

1. Abdal Dayem, A.; Hossain, M.K.; Lee, S.B.; Kim, K.; Saha, S.K.; Yang, G.M.; Choi, H.Y.; Cho, S.G. The Role of Reactive Oxygen Species (ROS) in the Biological Activities of Metallic Nanoparticles. *Int. J. Mol. Sci.* **2017**, *18*, 120. [CrossRef] [PubMed]
2. Warszyńska, M.; Repetowski, P.; Dąbrowski, J.M. Photodynamic therapy combined with immunotherapy: Recent advances and future research directions. *Coord. Chem. Rev.* **2023**, *495*, 215350. [CrossRef]
3. Pucelik, B.; Dąbrowski, J.M. Chapter Three—Photodynamic inactivation (PDI) as a promising alternative to current pharmaceuticals for the treatment of resistant microorganisms. In *Advances in Inorganic Chemistry*; van Eldik, R., Hubbard, C.D., Eds.; Academic Press: Cambridge, MA, USA, 2022; Volume 79, pp. 65–108.
4. Ma, H.-Y.; Zhao, L.; Guo, L.-H.; Zhang, H.; Chen, F.-J.; Yu, W.-C. Roles of reactive oxygen species (ROS) in the photocatalytic degradation of pentachlorophenol and its main toxic intermediates by TiO_2/UV. *J. Hazard. Mater.* **2019**, *369*, 719–726. [CrossRef] [PubMed]
5. Josefsen, L.B.; Boyle, R.W. Unique diagnostic and therapeutic roles of porphyrins and phthalocyanines in photodynamic therapy, imaging and theranostics. *Theranostics* **2012**, *2*, 916–966. [CrossRef] [PubMed]
6. Rybicka-Jasińska, K.; Wdowik, T.; Łuczak, K.; Wierzba, A.J.; Drapała, O.; Gryko, D. Porphyrins as Promising Photocatalysts for Red-Light-Induced Functionalizations of Biomolecules. *ACS Org. Inorg. Au* **2022**, *2*, 422–426. [CrossRef]
7. Chen, Y.; Li, A.; Huang, Z.-H.; Wang, L.-N.; Kang, F. Porphyrin-Based Nanostructures for Photocatalytic Applications. *Nanomaterials* **2016**, *6*, 51. [CrossRef]
8. Macdonald, I.J.; Dougherty, T.J. Basic principles of photodynamic therapy. *J. Porphyr. Phthalocyanines* **2001**, *5*, 105–129. [CrossRef]
9. Sternberg, E.D.; Dolphin, D.; Brückner, C. Porphyrin-based photosensitizers for use in photodynamic therapy. *Tetrahedron* **1998**, *54*, 4151–4202. [CrossRef]
10. McCleverty, J.A. *Comprehensive Coordination Chemistry II*; Elsevier Ltd.: Amsterdam, The Netherlands, 2003.
11. Luciano, M.; Brückner, C. Modifications of Porphyrins and Hydroporphyrins for Their Solubilization in Aqueous Media. *Molecules* **2017**, *22*, 980. [CrossRef]
12. Castro, K.A.D.F.; Moura, N.M.M.; Simões, M.M.Q.; Mesquita, M.M.Q.; Ramos, L.C.B.; Biazzotto, J.C.; Cavaleiro, J.A.S.; Faustino, M.A.F.; Neves, M.G.P.M.S.; da Silva, R.S. A Comparative Evaluation of the Photosensitizing Efficiency of Porphyrins, Chlorins and Isobacteriochlorins toward Melanoma Cancer Cells. *Molecules* **2023**, *28*, 4716. [CrossRef]
13. Pucelik, B.; Paczyński, R.; Dubin, G.; Pereira, M.M.; Arnaut, L.G.; Dąbrowski, J.M. Properties of halogenated and sulfonated porphyrins relevant for the selection of photosensitizers in anticancer and antimicrobial therapies. *PLoS ONE* **2017**, *12*, e0185984. [CrossRef] [PubMed]
14. Pucelik, B.; Sułek, A.; Drozd, A.; Stochel, G.; Pereira, M.M.; Pinto, S.M.A.; Arnaut, L.G.; Dąbrowski, J.M. Enhanced Cellular Uptake and Photodynamic Effect with Amphiphilic Fluorinated Porphyrins: The Role of Sulfoester Groups and the Nature of Reactive Oxygen Species. *Int. J. Mol. Sci.* **2020**, *21*, 2786. [CrossRef] [PubMed]
15. Singh, K.R.; Nayak, V.; Singh, J.; Singh, A.K.; Singh, R.P. Potentialities of bioinspired metal and metal oxide nanoparticles in biomedical sciences. *RSC Adv.* **2021**, *11*, 24722–24746. [CrossRef] [PubMed]
16. Fujishima, A.; Rao, T.N.; Tryk, D.A. Titanium dioxide photocatalysis. *J. Photochem. Photobiol. C Photochem. Rev.* **2000**, *1*, 1–21. [CrossRef]

17. Fagiolari, L.; Bonomo, M.; Cognetti, A.; Meligrana, G.; Gerbaldi, C.; Barolo, C.; Bella, F. Photoanodes for Aqueous Solar Cells: Exploring Additives and Formulations Starting from a Commercial TiO_2 Paste. *ChemSusChem* **2020**, *13*, 6562–6573. [CrossRef]

18. Bonomo, M.; Gatti, D.; Barolo, C.; Dini, D. Effect of Sensitization on the Electrochemical Properties of Nanostructured NiO. *Coatings* **2018**, *8*, 232. [CrossRef]

19. Cavallo, C.; Di Pascasio, F.; Latini, A.; Bonomo, M.; Dini, D. Nanostructured Semiconductor Materials for Dye-Sensitized Solar Cells. *J. Nanomater.* **2017**, *2017*, 5323164. [CrossRef]

20. Pandit, C.; Roy, A.; Ghotekar, S.; Khusro, A.; Islam, M.N.; Emran, T.B.; Lam, S.E.; Khandaker, M.U.; Bradley, D.A. Biological agents for synthesis of nanoparticles and their applications. *J. King Saud Univ.—Sci.* **2022**, *34*, 101869. [CrossRef]

21. Tuchina, E.; Tuchin, V. TiO_2 nanoparticle enhanced photodynamic inhibition of pathogens. *Laser Phys. Lett.* **2010**, *7*, 607–612. [CrossRef]

22. Li, Q.; Ni, Z.; Gong, J.; Zhu, D.; Zhu, Z. Carbon nanotubes coated by carbon nanoparticles of turbostratic stacked graphenes. *Carbon* **2008**, *46*, 434–439. [CrossRef]

23. Wu, S.; Weng, Z.; Liu, X.; Yeung, K.W.K.; Chu, P.K. Functionalized TiO_2 Based Nanomaterials for Biomedical Applications. *Adv. Funct. Mater.* **2014**, *24*, 5464–5481. [CrossRef]

24. Arun, J.; Nachiappan, S.; Rangarajan, G.; Alagappan, R.P.; Gopinath, K.P.; Lichtfouse, E. Synthesis and application of titanium dioxide photocatalysis for energy, decontamination and viral disinfection: A review. *Environ. Chem. Lett.* **2023**, *21*, 339–362. [CrossRef] [PubMed]

25. Jézéquel, H.; Chu, K.H. Enhanced adsorption of arsenate on titanium dioxide using Ca and Mg ions. *Environ. Chem. Lett.* **2005**, *3*, 132–135. [CrossRef]

26. Toma, F.; Bertrand, G.; Klein, D.; Coddet, C. Photocatalytic removal of nitrogen oxides via titanium dioxide. *Environ. Chem. Lett.* **2004**, *2*, 117–121. [CrossRef]

27. Lyu, J.; Zhu, L.; Burda, C. Considerations to improve adsorption and photocatalysis of low concentration air pollutants on TiO_2. *Catal. Today* **2014**, *225*, 24–33. [CrossRef]

28. Gilja, V.; Novaković, K.; Travas-Sejdic, J.; Hrnjak-Murgić, Z.; Kraljić Roković, M.; Žic, M. Stability and Synergistic Effect of Polyaniline/TiO_2 Photocatalysts in Degradation of Azo Dye in Wastewater. *Nanomaterials* **2017**, *7*, 412. [CrossRef]

29. Nguyen, T.P.; Nguyen, D.L.T.; Nguyen, V.H.; Le, T.H.; Vo, D.N.; Trinh, Q.T.; Bae, S.R.; Chae, S.Y.; Kim, S.Y.; Le, Q.V. Recent Advances in TiO(2)-Based Photocatalysts for Reduction of CO(2) to Fuels. *Nanomaterials* **2020**, *10*, 337. [CrossRef]

30. Dikkar, H.; Kapre, V.; Diwan, A.; Sekar, S. Titanium dioxide as a photocatalyst to create self-cleaning concrete. *Mater. Today Proc.* **2021**, *45*, 4058–4062. [CrossRef]

31. Sharifi, T.; Mohammadi, T.; Momeni, M.M.; Kusic, H.; Kraljic Rokovic, M.; Loncaric Bozic, A.; Ghayeb, Y. Influence of Photo-Deposited Pt and Pd onto Chromium Doped TiO_2 Nanotubes in Photo-Electrochemical Water Splitting for Hydrogen Generation. *Catalysts* **2021**, *11*, 212. [CrossRef]

32. Çeşmeli, S.; Biray Avci, C. Application of titanium dioxide (TiO_2) nanoparticles in cancer therapies. *J. Drug Target.* **2019**, *27*, 762–766. [CrossRef]

33. Dharma, H.N.C.; Jaafar, J.; Widiastuti, N.; Matsuyama, H.; Rajabsadeh, S.; Othman, M.H.D.; Rahman, M.A.; Jafri, N.N.M.; Suhaimin, N.S.; Nasir, A.M.; et al. A Review of Titanium Dioxide (TiO_2)-Based Photocatalyst for Oilfield-Produced Water Treatment. *Membranes* **2022**, *12*, 345. [CrossRef] [PubMed]

34. Radić, G.; Perović, K.; Sharifi, T.; Kušić, H.; Kovačić, M.; Kraljić Roković, M. Electrochemical Characterisation of the Photoanode Containing TiO_2 and SnS_2 in the Presence of Various Pharmaceuticals. *Catalysts* **2023**, *13*, 909. [CrossRef]

35. dela Rosa, F.M.; Popović, M.; Papac Zjačić, J.; Radić, G.; Kraljić Roković, M.; Kovačić, M.; Farré, M.J.; Genorio, B.; Lavrenčič Štangar, U.; Kušić, H.; et al. Visible-Light Activation of Persulfate or H_2O_2 by Fe_2O_3/TiO_2 Immobilized on Glass Support for Photocatalytic Removal of Amoxicillin: Mechanism, Transformation Products, and Toxicity Assessment. *Nanomaterials* **2022**, *12*, 4328. [CrossRef] [PubMed]

36. Schneider, J.; Matsuoka, M.; Takeuchi, M.; Zhang, J.; Horiuchi, Y.; Anpo, M.; Bahnemann, D.W. Understanding TiO_2 Photocatalysis: Mechanisms and Materials. *Chem. Rev.* **2014**, *114*, 9919–9986. [CrossRef] [PubMed]

37. Kuncewicz, J.; Ząbek, P.; Kruczała, K.; Szaciłowski, K.; Macyk, W. Photocatalysis Involving a Visible Light-Induced Hole Injection in a Chromate(VI)–TiO_2 System. *J. Phys. Chem. C* **2012**, *116*, 21762–21770. [CrossRef]

38. Yu, X.; Hou, T.; Li, Y.; Sun, X.; Lee, S.T. Effective band gap reduction of titanium oxide semiconductors by codoping from first-principles calculations. *Int. J. Quantum Chem.* **2013**, *113*, 2546–2553. [CrossRef]

39. Lim, J.; Bokare, A.D.; Choi, W. Visible light sensitization of TiO_2 nanoparticles by a dietary pigment, curcumin, for environmental photochemical transformations. *RSC Adv.* **2017**, *7*, 32488–32495. [CrossRef]

40. He, J.; Hagfeldt, A.; Lindquist, S.-E.; Grennberg, H.; Korodi, F.; Sun, L.; Åkermark, B. Phthalocyanine-Sensitized Nanostructured TiO_2 Electrodes Prepared by a Novel Anchoring Method. *Langmuir* **2001**, *17*, 2743–2747. [CrossRef]

41. Castro, K.A.D.F.; Moura, N.M.M.; Figueira, F.; Ferreira, R.I.; Simões, M.M.Q.; Cavaleiro, J.A.S.; Faustino, M.A.F.; Silvestre, A.J.D.; Freire, C.S.R.; Tomé, J.P.C.; et al. New Materials Based on Cationic Porphyrins Conjugated to Chitosan or Titanium Dioxide: Synthesis, Characterization and Antimicrobial Efficacy. *Int. J. Mol. Sci.* **2019**, *20*, 2522. [CrossRef]

42. Pumiglia, D.; Giustini, M.; Dini, D.; Decker, F.; Lanuti, A.; Mastroianni, S.; Veyres, S.; Caprioli, F. Photoelectrochemical Response of DSSCs under Prolonged Reverse Bias and Conduction Band Lowering in Ru-Complex-Sensitized TiO_2. *ChemElectroChem* **2014**, *1*, 1388–1394. [CrossRef]

43. Porcu, S.; Secci, F.; Ricci, P.C. Advances in Hybrid Composites for Photocatalytic Applications: A Review. *Molecules* **2022**, *27*, 6828. [CrossRef] [PubMed]

44. Ziental, D.; Czarczynska-Goslinska, B.; Mlynarczyk, D.T.; Glowacka-Sobotta, A.; Stanisz, B.; Goslinski, T.; Sobotta, L. Titanium Dioxide Nanoparticles: Prospects and Applications in Medicine. *Nanomaterials* **2020**, *10*, 387. [CrossRef] [PubMed]

45. Etacheri, V.; Di Valentin, C.; Schneider, J.; Bahnemann, D.; Pillai, S.C. Visible-light activation of TiO_2 photocatalysts: Advances in theory and experiments. *J. Photochem. Photobiol. C Photochem. Rev.* **2015**, *25*, 1–29. [CrossRef]

46. Hlabangwane, K.; Matshitse, R.; Managa, M.; Nyokong, T. The application of $Sn(IV)Cl_2$ and $In(III)Cl$ porphyrin-dyed TiO_2 nanofibers in photodynamic antimicrobial chemotherapy for bacterial inactivation in water. *Photodiagnosis Photodyn. Ther.* **2023**, *44*, 103795. [CrossRef] [PubMed]

47. Navidpour, A.H.; Abbasi, S.; Li, D.; Mojiri, A.; Zhou, J.L. Investigation of Advanced Oxidation Process in the Presence of TiO_2 Semiconductor as Photocatalyst: Property, Principle, Kinetic Analysis, and Photocatalytic Activity. *Catalysts* **2023**, *13*, 232. [CrossRef]

48. Pavel, M.; Anastasescu, C.; State, R.-N.; Vasile, A.; Papa, F.; Balint, I. Photocatalytic degradation of organic and inorganic pollutants to harmless end products: Assessment of practical application potential for water and air cleaning. *Catalysts* **2023**, *13*, 380. [CrossRef]

49. Sułek, A.; Pucelik, B.; Kuncewicz, J.; Dubin, G.; Dąbrowski, J.M. Sensitization of TiO_2 by halogenated porphyrin derivatives for visible light biomedical and environmental photocatalysis. *Catal. Today* **2019**, *335*, 538–549. [CrossRef]

50. Jiang, X.; Manawan, M.; Feng, T.; Qian, R.; Zhao, T.; Zhou, G.; Kong, F.; Wang, Q.; Dai, S.; Pan, J.H. Anatase and rutile in evonik aeroxide P25: Heterojunctioned or individual nanoparticles? *Catal. Today* **2018**, *300*, 12–17. [CrossRef]

51. Hantusch, M.; Bessergenev, V.; Mateus, M.C.; Knupfer, M.; Burkel, E. Electronic properties of photocatalytic improved Degussa P25 titanium dioxide powder. *Catal. Today* **2018**, *307*, 111–118. [CrossRef]

52. Yasin, S.A.; Abbas, J.A.; Ali, M.M.; Saeed, I.A.; Ahmed, I.H. Methylene blue photocatalytic degradation by TiO_2 nanoparticles supported on PET nanofibres. *Mater. Today Proc.* **2020**, *20*, 482–487. [CrossRef]

53. Modi, S.; Yadav, V.K.; Gacem, A.; Ali, I.H.; Dave, D.; Khan, S.H.; Yadav, K.K.; Rather, S.-U.; Ahn, Y.; Son, C.T.; et al. Recent and Emerging Trends in Remediation of Methylene Blue Dye from Wastewater by Using Zinc Oxide Nanoparticles. *Water* **2022**, *14*, 1749. [CrossRef]

54. Krishnan, S.; Shriwastav, A. Application of TiO_2 nanoparticles sensitized with natural chlorophyll pigments as catalyst for visible light photocatalytic degradation of methylene blue. *J. Environ. Chem. Eng.* **2021**, *9*, 104699. [CrossRef]

55. Hışır, A.; Karaoğlan, G.K.; Avcıata, O. Synthesis of tetracarboxy phthalocyanines modified TiO_2 nanocomposite photocatalysts and investigation of photocatalytic decomposition of organic pollutant methylene blue under visible light. *J. Mol. Struct.* **2022**, *1266*, 133498. [CrossRef]

56. Han, J.; Deng, Y.; Li, N.; Chen, D.; Xu, Q.; Li, H.; He, J.; Lu, J. A π-π stacking perylene imide/Bi_2WO_6 hybrid with dual transfer approach for enhanced photocatalytic degradation. *J. Colloid Interface Sci.* **2021**, *582*, 1021–1032. [CrossRef]

57. Houas, A.; Lachheb, H.; Ksibi, M.; Elaloui, E.; Guillard, C.; Herrmann, J.-M. Photocatalytic degradation pathway of methylene blue in water. *Appl. Catal. B Environ.* **2001**, *31*, 145–157. [CrossRef]

58. Xu, C.; Rangaiah, G.P.; Zhao, X.S. Photocatalytic Degradation of Methylene Blue by Titanium Dioxide: Experimental and Modeling Study. *Ind. Eng. Chem. Res.* **2014**, *53*, 14641–14649. [CrossRef]

59. Kim, M.G.; Lee, J.E.; Kim, K.S.; Kang, J.M.; Lee, J.H.; Kim, K.H.; Cho, M.; Lee, S.G. Photocatalytic degradation of methylene blue under UV and visible light by brookite–rutile bi-crystalline phase of TiO_2. *New J. Chem.* **2021**, *45*, 3485–3497. [CrossRef]

60. Mahy, J.G.; Douven, S.; Hollevoet, J.; Body, N.; Haynes, T.; Hermans, S.; Lambert, S.D.; Paez, C.A. Easy stabilization of Evonik Aeroxide P25 colloidal suspension by 4-hydroxybenzoic acid functionalization. *Surf. Interfaces* **2021**, *27*, 101501. [CrossRef]

61. Kroeze, J.E.; Savenije, T.J.; Warman, J.M. Efficient Charge Separation in a Smooth-TiO_2/Palladium-Porphyrin Bilayer via Long-Distance Triplet-State Diffusion. *Adv. Mater.* **2002**, *14*, 1760–1763. [CrossRef]

62. Zabel, P.; Dittrich, T.; Funes, M.; Durantini, E.N.; Otero, L. Charge Separation at Pd−Porphyrin/TiO_2 Interfaces. *J. Phys. Chem. C* **2009**, *113*, 21090–21096. [CrossRef]

63. Pasternack, R.F.; Francesconi, L.; Raff, D.; Spiro, E. Aggregation of nickel (II), copper (II), and zinc (II) derivatives of water-soluble porphyrins. *Inorg. Chem.* **1973**, *12*, 2606–2611. [CrossRef]

64. Occhiuto, I.G.; Castriciano, M.A.; Trapani, M.; Zagami, R.; Romeo, A.; Pasternack, R.F.; Monsù Scolaro, L.; Controlling, J. Aggregates Formation and Chirality Induction through Demetallation of a Zinc(II) Water Soluble Porphyrin. *Int. J. Mol. Sci.* **2020**, *21*, 4001. [CrossRef]

65. Dąbrowski, J.M.; Pucelik, B.; Pereira, M.M.; Arnaut, L.G.; Stochel, G. Towards tuning PDT relevant photosensitizer properties: Comparative study for the free and Zn^{2+} coordinated meso-tetrakis[2,6-difluoro-5-(N-methylsulfamylo)phenyl]porphyrin. *J. Coord. Chem.* **2015**, *68*, 3116–3134. [CrossRef]

66. Bonomo, M.; Dini, D. Nanostructured p-Type Semiconductor Electrodes and Photoelectrochemistry of Their Reduction Processes. *Energies* **2016**, *9*, 373. [CrossRef]

67. Macyk, W.; Burgeth, G.; Kisch, H. Photoelectrochemical properties of platinum(IV) chloride surface modified TiO2. *Photochem. Photobiol. Sci.* **2003**, *2*, 322–328. [CrossRef]

68. Tabari, T.; Łabuz, P.; Nowakowska, A.M.; Kobielusz, M.; Pacia, M.; Macyk, W. Studying the governing factors on the photo(electro)catalytic activity of surface-modified photocatalysts under visible light illumination. *Dye. Pigment.* **2023**, *213*, 111154. [CrossRef]

69. Hebda, M.; Stochel, G.; Szaciłowski, K.; Macyk, W. Optoelectronic Switches Based on Wide Band Gap Semiconductors. *J. Phys. Chem. B* **2006**, *110*, 15275–15283. [CrossRef]

70. Nosaka, Y.; Nosaka, A.Y. Generation and Detection of Reactive Oxygen Species in Photocatalysis. *Chem. Rev.* **2017**, *117*, 11302–11336. [CrossRef]

71. de Oliveira, C.P.M.; Lage, A.L.A.; Martins, D.C.d.S.; Mohallem, N.D.S.; Viana, M.M. High surface area TiO_2 nanoparticles: Impact of carboxylporphyrin sensitizers in the photocatalytic activity. *Surf. Interfaces* **2020**, *21*, 100774. [CrossRef]

72. Zuo, R.; Du, G.; Zhang, W.; Liu, L.; Liu, Y.; Mei, L.; Li, Z. Photocatalytic Degradation of Methylene Blue Using TiO_2 Impregnated Diatomite. *Adv. Mater. Sci. Eng.* **2014**, *2014*, 170148. [CrossRef]

73. Dąbrowski, J.M.; Pucelik, B.; Pereira, M.M.; Arnaut, L.G.; Macyk, W.; Stochel, G. New hybrid materials based on halogenated metalloporphyrins for enhanced visible light photocatalysis. *RSC Adv.* **2015**, *5*, 93252–93261. [CrossRef]